NANO LETTERS

pubs.acs.org/NanoLett

Letter

Nanoscale Visualization of a Photoinduced Plasmonic Near-Field in a Single Nanowire by Free Electrons

Dingguo Zheng, Siyuan Huang, Chunhui Zhu, Peng Xu, Zian Li, Hong Wang, Jun Li, Huanfang Tian, Huaixin Yang, and Jianqi Li*

Cite This: *Nano Lett.* 2021, 21, 10238–10243

Read Online

ACCESS | Metrics & More | Article Recommendations | Supporting Information

ABSTRACT: Swift electrons can undergo inelastic interactions not only with electrons but also with near-fields, which may result in an energy loss or gain. Developments in photon-induced near-field electron microscopy (PINEM) enable direct imaging of the plasmon near-field distribution with nanometer resolution. Here, we report an analysis of the surface plasmonic near-field structure based on PINEM observations of silver nanowires. Single-photon order-selected electron images revealed the wavelike and banded structure of electric equipotential regions for a confined near-field integral associated with typical absorption of photon quanta ($n\hbar\omega$). Multimodal plasmon oscillations and second-harmonic generation were simultaneously observed, and the polarization dependence of plasmon wavelength and symmetry properties were analyzed. Based on advanced imaging techniques, our work has implications for future studies of the localized-field structures at interfaces and visualization of novel phenomena in nanostructures, nanosensors, and plasmonic devices.

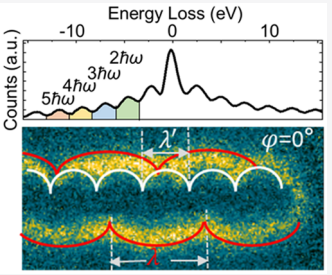

KEYWORDS: *photon-induced near-field electron microscopy, silver nanowire, plasmonic near-field, ultrafast transmission electron microscopy*

Ultrafast transmission electron microscopy (UTEM) has become a powerful tool for characterizing dynamic processes in physics, chemistry, materials science, and biology. Importantly, this technique offers the ability to visualize transient states of nanometer-sized objects.[1−3] Furthermore, when nanostructures are optically excited, photon-induced near-field electron microscopy (PINEM) that developed from UTEM can be used to directly observe the surface plasmon near-field structure with high spatiotemporal resolution.[4−7] In UTEM, near-relativistic electrons not only interact with the specimen, but also the near-field generated by photoexcited collective electrons in nanomaterials. In particular, swift electrons strongly interact with the confined evanescent near-field, yielding characteristic inelastic scattered electrons, as detected in PINEM investigations.[8,9]

For a silver nanowire, surface plasmon polaritons (SPPs) can be excited and propagate along the axial direction.[10] Certain fundamental structural features of SPPs have been observed by scanning near-field optical microscopy,[11] electron energy-loss spectroscopy (EELS),[12] photoemission electron microscopy,[13] etc. In PINEM observations, plasmonic near-fields can be detected with nanoscale spatial resolution at the femtosecond time scale in nanomaterials, such as nanoparticles,[14,15] nanowires,[5,16] graphene strips,[17] and silver mirrors.[18,19] However, direct imaging of the near-field distribution with an energy window with single-photon order has never been achieved. Furthermore, no nonlinear feature of SPPs has been experimentally revealed by PINEM.

Here, we report an extensive study of the surface plasmon near-field structure based on PINEM observations of silver nanowires. Single-photon order-selected electron images (SPOSEIs), i.e., energy-filtered imaging with a width only a single photon energy, revealed that wavelike and banded structures of the near field were associated with absorption of a specific number of photon quanta. In addition, multimodal plasmon oscillations and second-harmonic generation (SHG) were simultaneously observed at a high pump power density. We also analyzed the optical polarization dependence of the SPP wavelength and asymmetric distribution of the near field.

A schematic diagram of the UTEM setup used for investigation of a silver nanowire after femtosecond-pulsed laser excitation is shown in Figure 1a. This setup was based on a microscope fitted with a Schottky-type field-emission gun.[20] This setup could operate in continuous or pulsed mode, and electron-pulse emission was achieved by integrating a laser port between the electron gun and the TEM column. The left panel of Figure 1a shows an enlarged view of a specimen in the modified UTEM chamber, in which interactions took place between the femtosecond-pulsed laser, swift electrons and the silver nanowire. In previous studies, it has been established that

Received: August 18, 2021
Revised: November 25, 2021
Published: December 3, 2021

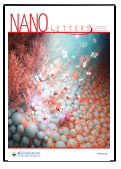

https://doi.org/10.1021/acs.nanolett.1c03203
Nano Lett. 2021, 21, 10238−10243

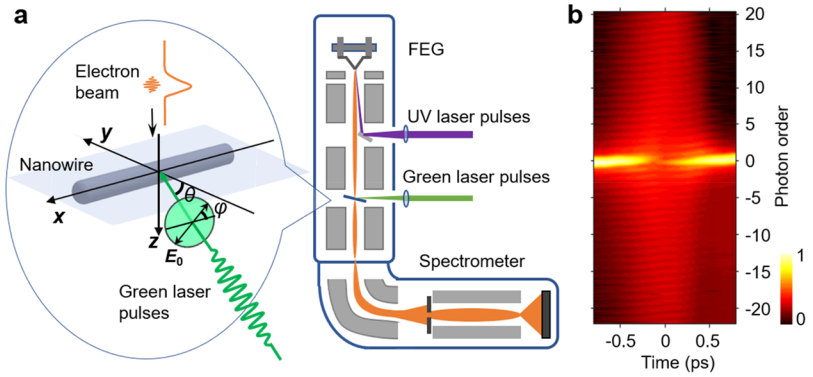

Figure 1. Schematic illustration of the ultrafast transmission electron microscopy (UTEM) apparatus and electron energy-loss spectroscopy (EELS) data for pulsed-electrons interacting with the plasmon near-field. (a) Schematic diagrams of the optical and electric components of the UTEM system. (left) Electron−specimen interaction and the optical pump beam for exciting surface-plasmon oscillations in the specimen. Electron emission in the UTEM system from a tungsten filament was driven by femtosecond laser pulses (wavelength: 257 nm), and the specimen was also illuminated by femtosecond pulses (wavelength: 515 nm). (b) Electron populations in different quantum states revealed by time-resolved EELS for a silver nanowire.

pulsed electrons via the optical near field can be strongly modulated by absorbing or emitting photons with energy quanta of $n\hbar\omega$, where n is an integer, $\hbar$ is the reduced Planck constant, and ω is the photon frequency of the pump laser.[5,6,21] Energy levels exist in ladder states spaced by the photon energy of $\hbar\omega$, and the population of electrons in energy level is visibly modulated by strong electron−photon coupling,[6,8,9] as observed in time-resolved EELS spectroscopy (Figure 1b). A strong plasmon near field modulates free electrons to form an electron energy comb, where each energy state has a slight slip owing to dispersive propagation of the electron pulse.[22] This is because the lower-energy electrons interact with the near field earlier than the higher-energy electrons in the pump−probe framework.

The PINEM images obtained from light with normal incidence ($\theta = 0$) are shown in Figure S1. It exhibited a wavelike structure when the external instantaneous electric field was parallel to silver nanowire (Figure S1a) and was uniform when the electric field was perpendicular to the nanowire (Figure S1b), which is consistent with previous reports.[5,16,23−25] The wavelike structure in Figure S1a can be acknowledged as an SPP standing wave, which is a basic surface plasmon mode with $m = 0$ (TM_0 mode),[10] further analysis shown in Figure S2. In previous studies of nanosystems and related nanodevices, interactions between photons and electrons have shown to be related to the near field on a scale comparable with the optical wavelength. Moreover, interactions between swift electrons and the optical near field in UTEM can be expressed by a quantum mechanical multilevel system.[6,7,25,26]

Figure 2a shows typical EELS results from a silver nanowire irradiated with a femtosecond-laser beam, illustrating the presence of a spectral comb with multiple sidebands arising from photon absorption or emission. Measurements of the energy-filtered images of a specific quantum state can simultaneously provide insight into the spatial distribution of the plasmon field and its correlation with spectral features. Here, using a newly developed field-assisted UTEM system, we achieved SPOSEIs with an energy window of 2.4 eV for the energy states of $n = 2$, 3, 4, and 5, as indexed in Figure 2a. In comparison with the method using electron beam scanning to record local spectra,[4,27,28] here quantitative imaging individual photon quantum states was achieved by energy-filtered images with single photon energy resolution. It should be an efficient method to reveal near-field distribution of nanomaterials upon laser excitation. As shown in Figure 2c, these images reveal the spatial alteration and microdomains of a selected quantum state. For example, a high energy state is typically excited in regions neighboring the nanowire surface, and adjacent quantum states overlap slightly in the PINEM images. In Figure S3, we show theoretical SPOSEIs, which exhibit the same characteristics. By contrast, the PINEM images obtained by collecting multiorder electrons (Figure 2d) (energy window from −3.6 to −50 eV) and the results reported in the literature[5,14−17,24] cannot distinguish each photon order state distribution, only contained mixed characteristics.

The banded structural features specifically assigned to the quantum states can be regarded as the electric equipotential regions for a confined near-field integral. This is because the probabilities of electrons being in the quantum state $|n\rangle$ can be determined from the near-field integral $|\beta|$ at the (x, y) position:[6,25,26]

$$P_n(x, y) = J_n^2(2|\beta(x, y)|)$$

where β is the spatial integral of the near-field of the z-component:

$$\beta(x, y) = \frac{e}{\hbar\omega}\int_{-\infty}^{\infty} dz\, E_z(x, y, z)e^{-i\omega z/v}$$

Here J_n is a Bessel function of the first kind with the order n; e is the elementary charge; and v is the electron speed. Figure 2b presents the theoretical multiorder spectral sideband occupation obtained by the interaction of electrons with a uniform near field. It can be seen that the spatial location of a certain quantum state is dependent on the specific near-field strength. For example, the electron image with a gain of $2\hbar\omega$ indicates the distribution of the near-field integral (β), which has a strength of approximately 1.53, corresponding to an electric potential ($\left|\int_{-\infty}^{\infty} dz\, E_z(x, y, z)e^{-i\omega z/v}\right|$) of approximately 1.83 V in our experiments. We note that another $2\hbar\omega$ gain peak should theoretically appear at 3.35 (as indicated by the arrow in Figure 2b). However, this was not observed in the image, which is possibly because of the sharp increase of the near field close to the nanowire and the limited spatial resolution of the UTEM system. A more detailed analysis of the near field in the

https://doi.org/10.1021/acs.nanolett.1c03203
Nano Lett. 2021, 21, 10238−10243

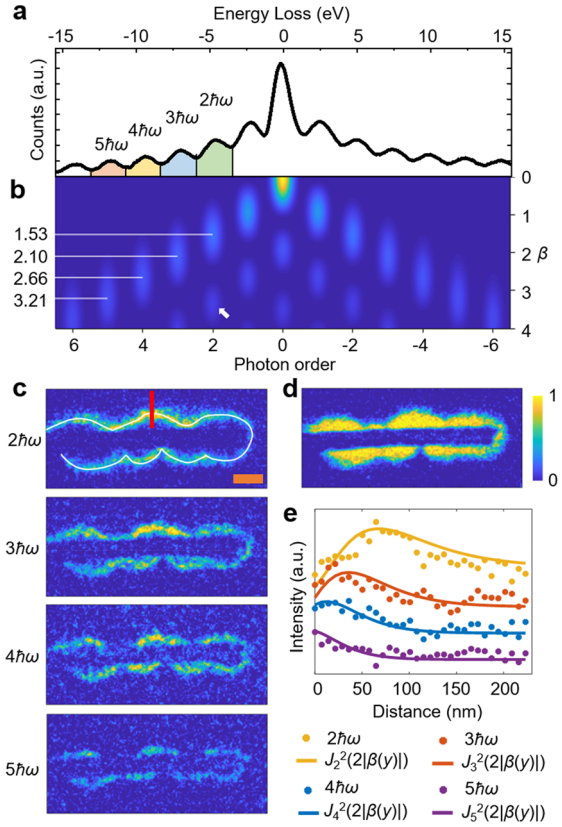

Figure 2. Spectrum and electron images of the plasmon near field on a silver nanowire at φ = 50°. (a) Electron energy-loss spectroscopy data showing multiple photon absorption and emission. The four colored areas represent the energy ranges of the imaging electrons that formed the patterns in c. (b) Theoretical result of *n*-photon order occupation as a function of near-field strength. The white lines on the left indicate the first maximum for photon occupation numbers from 2 to 5. (c) Single-photon order-selected electron images illustrating the electron population of quantum energy states arising from electron−photon interactions of the nanowire. The white line in the $2\hbar\omega$ image was obtained by connecting the maximum value of counts in the normal direction of nanowire. This line represents the electric equipotential plane of β = 1.53. Nanowire diameter 110 nm; energy window 2.4 eV; scale bar 100 nm. (d) Photon-induced near-field electron microscopy image obtained from the energy-gain region of −3.6 to −50 eV. (e) Intensity profile in the direction perpendicular to the nanowire axis (obtained by integrating the region indicated by the red line in c and the same region in other images of c). The theoretical results were obtained by considering that the intensity of the near field decays exponentially with distance from the nanowire.

direction perpendicular to the nanowire axis is shown in Figure 2e. The profile of the population for each examined quantum order was reproduced by the Bessel function of the first kind. These results predict that the population in each photon state will show oscillation in real space, if existence of an enough strength and smooth distribution near field.

The fundamental properties of the field strength with visible spectral modifications have also been discussed based on the coherent manipulation of quantum states of the respective level amplitudes with multilevel Rabi oscillations.[6,7,26] However, the SPOSEIs in our study provide a quantitative tool that could be employed in coherently control experiments and clearly reveal the microstructural features of plasmonic near fields, paving the way to coherently manipulate the quantum state of the free-electron population in subnanoscale space.

Selection of specific quantum state electrons could reveal finer structure of the near-field, but the intensities in the images are pretty low. Therefore, considering both accuracy and intensity, we selected a few quantum states for imaging. Figure 3b−e shows a series PINEM images with an electron

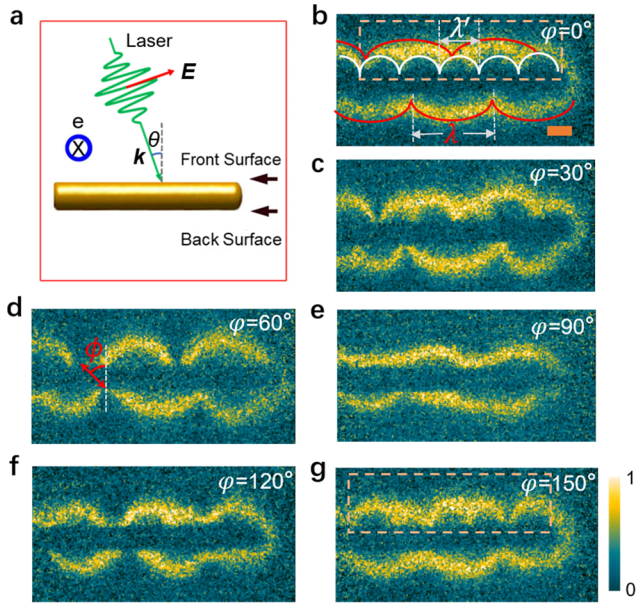

Figure 3. Partial photon order-selected electron images of a silver nanowire at an incident angle θ = 24°. (a) Top view of side-entry laser illumination, where pump laser is perpendicular to the electron beam. (b−g) Series of PINEM images with electron energies encompassing quantum states from −3.6 to −13.2 eV (i.e., n = 2−5) corresponding the different optical polarizations (φ), as indicated in the top right of the images. φ = 0° represents optical polarization in the x−y plane. Electrons in high energy states (n > 5) were filtered out, resulting in low contrast near the nanowire. The red and white curves with different periods in φ = 0° indicate two different modes on the front surface: λ = 385 ± 10 nm, λ' = 175 ± 6 nm. The brown rectangles in Figure 3b,g indicate a minor mode that always had five periods regardless of light polarization. The intensity of the minor mode changed rapidly upon altering the polarization: nanowire diameter 110 nm; scale bar 100 nm.

energy window within −3.6 to −13.2 eV (i.e., includes quantum state n = 2−5) for a sample excited with differential optical polarizations. These PINEM images are obtained with the pumping laser perpendicular to the electron beam as illustrated in Figure S4, and a top view of experimental scheme showed in Figure 3a. Electrons in high quantum states (n > 5) were filtered out, resulting in low contrast in the intense near-field region. Notably, the surface-plasmon waves and near-field distribution depended on the light polarization. For example, plasmonic waves had only a small fluctuation along the nanowire at φ = 90° (Figure 3e); by contrast, at φ = 60° or 120° (Figure 3d, Figure 3f) the PINEM image showed clear wave nodes. Those near-field patterns are fundamentally correlated with interference effects of plasmons and external light fields.[29] The full variation of the pattern upon rotation of the optical polarization is illustrated in Figure S5, and the unfiltered images of samples shown in Figure S6.

The distributions of the near field at the front and back surfaces differed. For example, plasmon oscillations with a relative short period typically appeared at the front surface (Figure 3b). In fact, two plasmonic oscillation modes were

https://doi.org/10.1021/acs.nanolett.1c03203
Nano Lett. 2021, 21, 10238−10243

revealed by the PINEM images: a major mode with a relatively long period, which is linear excited SPPs with fundamental frequency; and a minor mode with a short period (could be distinguished in Figure 3b,c,g), which we attribute to SHG. However, only the major mode was visible on the back surface, which suggests that a nanowire with a diameter of 110 nm has a different photoinduced near-field distribution between front and back surface, owing to optical absorption and scattering. Furthermore, it should be noted that the minor mode can only be observed with a relatively high pump laser power, and the high quantum state electrons are filtered out for PINEM imaging, e. g. Figure 3b−g are taken with the energy window include n = 2−5 electrons to exhibit the image contrast of SHG. But in Figure S1, the energy window includes all of energy-gain electrons.

Extensive examination of our experimental data revealed that the intensity of the minor plasmon mode often rapidly decreased to zero upon rotation of the polarization to the vertical direction. This polarization dependence is in good agreement with previous investigations and theoretical expectations for SHG.[30−32] The schematic illustration in Figure 4a is in the case of $\theta = 24°$ and $\varphi = 0°$, depicts the differences of the electric field and its z-component distribution between the front and back surfaces. This filed distribution is also in good agreement with those of previous works on SHG in nanorods and nanowires.[33,34] The periodicity of the minor modes is almost half that of the major mode. The measured minor mode wavelength was 175 ± 6 nm, and the major mode wavelength was 385 ± 10 nm at $\varphi = 0°$, which is in agreement with the theoretical analysis (see the Supporting Information). In our measurements, the maximum pump power density was ∼4.8 × 10^{10} W/cm^2 (power 150 mW; pulse duration 800 fs; spot size 50 μm diameter; reptation rate 200 kHz), which is comparable with values used in the literature,[35−37] and should be sufficiently strong to excite high-order harmonic generation, as estimated in the nonlinear optics.[38] It is noted that the appearance of SHG can be theoretically analyzed based on the asymmetric features in energy-loss spectra as reported by Konečná et al.[39] In another silver nanowire, we have exhibited the relevant spectra in Figure S7 of the Supporting Materials. A ∼15% local SHG intensity is estimated at an area very near surface of the nanowire, but the average fraction of SHG in all plasmon near fields could be much lower. Moreover, in order to confirm the existence of SHG, we have made a grating structure in which silver nanorods are arranged periodically along the electron beam direction. As a result, the asymmetric feature of spectrum appears in a large energy range. The main results of this grating structure will be reported in a paper in preparation.

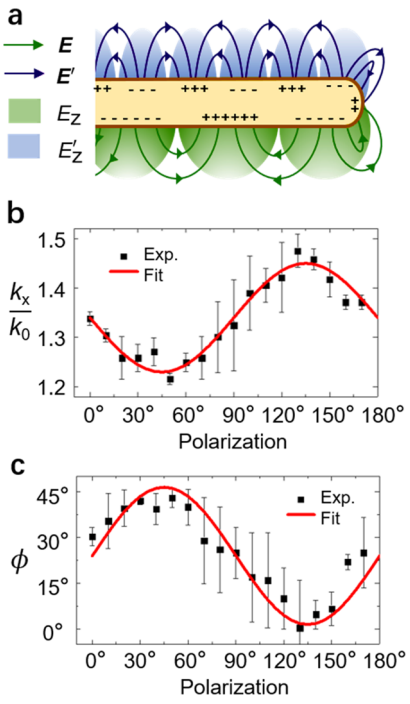

Figure 4. Schematic illustration of the electric-field distribution and changes in the pattern of surface plasmon polaritons (SPPs) as a function of polarization angle (φ) from 0° to 180°. (a) Electric-field distribution corresponding to the nanowire shown in Figure 3b. For the front surface, only distribution for the minor mode is plotted (E' and its z-component E'_z). For the back face, linear excitations of the SPP electric field (E and its z-component E_z) are plotted. (b) Variation of the surface plasmon wavevector of a major mode. Here, $k_x = \frac{2\pi}{\lambda}$, where λ is the period of the major mode (see Figure 3b) and k_0 is the wavevector of the external light. The curves in b and c were both fitted with sinusoidal functions. (c) Phase difference as a function of polarization angle. The phase difference was defined as the asymmetric degree of the plasmon near-field distribution on the two sides of the nanowire (marked as ϕ; $0° \le \phi \le 45°$; see Figure 3d). ϕ was measured as the angle formed by the radial plane of the nanowire and the line connecting one node to the nearest node on the opposite side of the nanowire.

Now we discuss the changes of the plasmon oscillation pattern for the major mode as the polarization direction (φ) was varied from 0° to 180°. SPPs strongly depend on the external electric-field vector and the plasmon near field will redistribute if there is a change in the direction of the electric-field vector.[10,40,41] According to classical electromagnetic theory, there are discrete modes of the electric field in the outer regions of the nanowire under light-excitation.[10,42,43] Considering a nanowire with a radius of 55 nm, only m = 0, ±1 modes can be excited (corresponding to TM_0, HE_1, and HE_{-1} modes),[41,43−45] and the wavevectors of three modes are slightly different. Because of the superposition of these modes and the phase difference among them, the wavevector of the major mode varies as a sine function when the polarization angle is changed from 0° to 180°, as shown in Figure 4b. Remarkably, the standing wave patterns of the plasmon field at the front and back surfaces yield a spatial phase difference (ϕ, indicated in Figure 3d), which also varies sinusoidally with polarization rotation (Figure 4c). k_x and ϕ have the opposite trend with respect to optical polarization. Because SPPs are the superposition of these modes, chiral SPPs can be generated on the nanowire.[41] Only when those modes have no phase difference (i.e., no phase retardation), the plasmon fields at the front and back of the nanowire are symmetric and the wavevectors reach their maxima ($\varphi \approx 135°$). When the mode phases are mismatched, chiral SPPs result in asymmetry distributions at the front and back surfaces. In this case, a longer distance is required to contain these modes, which results in a smaller wavevector.

In conclusion, we directly imaged the plasmon near-field distribution of a silver nanowire using Schottky-type field-emission UTEM. The excitations of plasmon oscillations and the distribution of the surface near-field strongly depended on the polarization of the pump laser. SPOSEIs revealed a banded structure of equipotential regions, which are associated with

https://doi.org/10.1021/acs.nanolett.1c03203
Nano Lett. 2021, 21, 10238−10243

typical absorption of photon quanta in real space. At high pump power densities, multimodal plasmon oscillations and SHG were observed. We believe that observations and analyses of the localized electric fields created within, or in the vicinity of, nanostructures will offer useful fundamental insight for photonic and plasmonic applications.

■ ASSOCIATED CONTENT

Supporting Information

The Supporting Information is available free of charge at https://pubs.acs.org/doi/10.1021/acs.nanolett.1c03203.

Details of experimental methods, simulation, analysis in the case of normal incident laser pump, and the dispersion relation of SPPs in nanowire. Additional data of the full variation of the pattern upon rotation of the optical polarization (PDF)

■ AUTHOR INFORMATION

Corresponding Author

Jianqi Li − *Beijing National Laboratory for Condensed Matter Physics, Institute of Physics, Chinese Academy of Sciences, Beijing 100190, China; School of Physical Sciences, University of Chinese Academy of Science, Beijing 100049, China; Yangtze River Delta Physics Research Center Co., Ltd., Liyang, Jiangsu 213300, China;* orcid.org/0000-0002-4808-6347; Email: ljq@aphy.iphy.ac.cn

Authors

Dingguo Zheng − *Beijing National Laboratory for Condensed Matter Physics, Institute of Physics, Chinese Academy of Sciences, Beijing 100190, China; School of Physical Sciences, University of Chinese Academy of Science, Beijing 100049, China;* orcid.org/0000-0002-7227-0048

Siyuan Huang − *Beijing National Laboratory for Condensed Matter Physics, Institute of Physics, Chinese Academy of Sciences, Beijing 100190, China; School of Physical Sciences, University of Chinese Academy of Science, Beijing 100049, China*

Chunhui Zhu − *Beijing National Laboratory for Condensed Matter Physics, Institute of Physics, Chinese Academy of Sciences, Beijing 100190, China*

Peng Xu − *Beijing National Laboratory for Condensed Matter Physics, Institute of Physics, Chinese Academy of Sciences, Beijing 100190, China*

Zian Li − *Beijing National Laboratory for Condensed Matter Physics, Institute of Physics, Chinese Academy of Sciences, Beijing 100190, China*

Hong Wang − *Beijing National Laboratory for Condensed Matter Physics, Institute of Physics, Chinese Academy of Sciences, Beijing 100190, China; School of Physical Sciences, University of Chinese Academy of Science, Beijing 100049, China*

Jun Li − *Beijing National Laboratory for Condensed Matter Physics, Institute of Physics, Chinese Academy of Sciences, Beijing 100190, China*

Huanfang Tian − *Beijing National Laboratory for Condensed Matter Physics, Institute of Physics, Chinese Academy of Sciences, Beijing 100190, China*

Huaixin Yang − *Beijing National Laboratory for Condensed Matter Physics, Institute of Physics, Chinese Academy of Sciences, Beijing 100190, China; School of Physical Sciences, University of Chinese Academy of Science, Beijing 100049, China; Yangtze River Delta Physics Research Center Co., Ltd., Liyang, Jiangsu 213300, China*

Complete contact information is available at: https://pubs.acs.org/10.1021/acs.nanolett.1c03203

Author Contributions

D.Z. designed and carried out the experiments, analyzed the results, and wrote the manuscript. Ji.L. conducted analysis and manuscript writing. C.Z., H.W., and Ju.L. contributed to the experiments and analysis. P.X., S.H., and Z.L. contributed to the simulations and theoretical analysis. H.T. and H.Y. contributed to writing the manuscript.

Notes

The authors declare no competing financial interest.

■ ACKNOWLEDGMENTS

This work was supported by the National Key Research and Development Program of China (Grant Nos. 2017YFA0504703, 2017YFA0302904), the Scientific Instrument Developing Project of the Chinese Academy of Sciences (Grant Nos. YJKYYQ20200055, ZDKYYQ2017000, 22017BA10), the Strategic Priority Research Program (B) of the Chinese Academy of Sciences (Grant Nos. XDB25000000, XDB33010100), the National Natural Science Foundation of China (Grant Nos. 11774391, 12074408), Beijing Municipal Science and Technology major project (Z201100001820006), IOP Hundred Talents Program (Grant Nos. Y9K5051), and the China Postdoctoral Science Foundation funded project (Grant No. BX20180351). We thank Adam Brotchie, Ph.D., from Liwen Bianji (Edanz) (https://www.liwenbianji.cn) for editing the language of a draft of this manuscript.

■ REFERENCES

(1) Shorokhov, D.; Zewail, A. H. Perspective: 4D ultrafast electron microscopy—Evolutions and revolutions. *J. Chem. Phys.* **2016**, *144*, 080901−080901a.

(2) Vanacore, G. M.; Fitzpatrick, A. W. P.; Zewail, A. H. Four-dimensional electron microscopy: Ultrafast imaging, diffraction and spectroscopy in materials science and biology. *Nano Today* **2016**, *11*, 228−249.

(3) Barwick, B.; Zewail, A. H. Photonics and Plasmonics in 4D Ultrafast Electron Microscopy. *ACS Photonics* **2015**, *2*, 1391−1402.

(4) Yurtsever, A.; van der Veen, R. M.; Zewail, A. H. Subparticle Ultrafast Spectrum Imaging in 4D Electron Microscopy. *Science* **2012**, *335*, 59−64.

(5) Barwick, B.; Flannigan, D. J.; Zewail, A. H. Photon-induced near-field electron microscopy. *Nature* **2009**, *462*, 902−906.

(6) Park, S. T.; Lin, M.; Zewail, A. H. Photon-induced near-field electron microscopy (PINEM): theoretical and experimental. *New J. Phys.* **2010**, *12*, 123028.

(7) Garcia de Abajo, F. J.; Asenjo-Garcia, A.; Kociak, M. Multiphoton absorption and emission by interaction of swift electrons with evanescent light fields. *Nano Lett.* **2010**, *10*, 1859−63.

(8) Dahan, R.; Nehemia, S.; Shentcis, M.; Reinhardt, O.; Adiv, Y.; Shi, X.; Be'er, O.; Lynch, M. H.; Kurman, Y.; Wang, K.; Kaminer, I. Resonant phase-matching between a light wave and a free-electron wavefunction. *Nat. Phys.* **2020**, *16*, 1123−1131.

(9) Kfir, O.; Lourenço-Martins, H.; Storeck, G.; Sivis, M.; Harvey, T. R.; Kippenberg, T. J.; Feist, A.; Ropers, C. Controlling free electrons with optical whispering-gallery modes. *Nature* **2020**, *582*, 46−49.

(10) Sarid, D.; Challener, W. A. *Modern Introduction to Surface Plasmons: Theory, Mathematica Modeling, and Applications*; Cambridge University Press: Cambridge, 2010.

(11) Dunn, R. C. Near-Field Scanning Optical Microscopy. *Chem. Rev.* **1999**, *99*, 2891−2928.

(12) Colliex, C.; Kociak, M.; Stéphan, O. Electron Energy Loss Spectroscopy imaging of surface plasmons at the nanometer scale. *Ultramicroscopy* **2016**, *162*, A1−A24.
(13) Kahl, P.; Wall, S.; Witt, C.; Schneider, C.; Bayer, D.; Fischer, A.; Melchior, P.; Horn-von Hoegen, M.; Aeschlimann, M.; Meyer zu Heringdorf, F.-J. Normal-Incidence Photoemission Electron Microscopy (NI-PEEM) for Imaging Surface Plasmon Polaritons. *Plasmonics* **2014**, *9*, 1401−1407.
(14) Yurtsever, A.; Zewail, A. H. Direct visualization of near-fields in nanoplasmonics and nanophotonics. *Nano Lett.* **2012**, *12*, 3334−3338.
(15) Yurtsever, A.; Baskin, J. S.; Zewail, A. H. Entangled nanoparticles: discovery by visualization in 4D electron microscopy. *Nano Lett.* **2012**, *12*, 5027−5032.
(16) Piazza, L.; Lummen, T. T.; Quinonez, E.; Murooka, Y.; Reed, B. W.; Barwick, B.; Carbone, F. Simultaneous observation of the quantization and the interference pattern of a plasmonic near-field. *Nat. Commun.* **2015**, *6*, 6407.
(17) Park, S. T.; Yurtsever, A.; Baskin, J. S.; Zewail, A. H. Graphene-layered steps and their fields visualized by 4D electron microscopy. *Proc. Natl. Acad. Sci. U. S. A.* **2013**, *110*, 9277−82.
(18) Vanacore, G. M.; Madan, I.; Berruto, G.; Wang, K.; Pomarico, E.; Lamb, R. J.; McGrouther, D.; Kaminer, I.; Barwick, B.; Garcia de Abajo, F. J.; Carbone, F. Attosecond coherent control of free-electron wave functions using semi-infinite light fields. *Nat. Commun.* **2018**, *9*, 2694.
(19) Vanacore, G. M.; Berruto, G.; Madan, I.; Pomarico, E.; Biagioni, P.; Lamb, R. J.; McGrouther, D.; Reinhardt, O.; Kaminer, I.; Barwick, B.; Larocque, H.; Grillo, V.; Karimi, E.; Garcia de Abajo, F. J.; Carbone, F. Ultrafast generation and control of an electron vortex beam via chiral plasmonic near fields. *Nat. Mater.* **2019**, *18*, 573−579.
(20) Zhu, C.; Zheng, D.; Wang, H.; Zhang, M.; Li, Z.; Sun, S.; Xu, P.; Tian, H.; Li, Z.; Yang, H.; Li, J. Development of analytical ultrafast transmission electron microscopy based on laser-driven Schottky field emission. *Ultramicroscopy* **2020**, *209*, 112887.
(21) Rossouw, D.; Couillard, M.; Vickery, J.; Kumacheva, E.; Botton, G. A. Multipolar plasmonic resonances in silver nanowire antennas imaged with a subnanometer electron probe. *Nano Lett.* **2011**, *11*, 1499−504.
(22) Park, S. T.; Kwon, O.-H.; Zewail, A. H. Chirped imaging pulses in four-dimensional electron microscopy: femtosecond pulsed hole burning. *New J. Phys.* **2012**, *14*, 053046.
(23) Pomarico, E.; Madan, I.; Berruto, G.; Vanacore, G. M.; Wang, K.; Kaminer, I.; Abajo, F. J. G. d.; Carbone, F. meV Resolution in Laser-Assisted Energy-Filtered Transmission Electron Microscopy. *ACS Photonics* **2018**, *5* (3), 759−764.
(24) Lummen, T. T. A.; Lamb, R. J.; Berruto, G.; Lagrange, T.; Negro, L. D.; Abajo, F. J. G. d.; McGrouther, D.; Barwick, B.; Carbone, F. Imaging and controlling plasmonic interference fields at buried interfaces. *Nat. Commun.* **2016**, *7* (1), 13156.
(25) Park, S. T.; Zewail, A. H. Photon-induced near-field electron microscopy: Mathematical formulation of the relation between the experimental observables and the optically driven charge density of nanoparticles. *Phys. Rev. A: At., Mol., Opt. Phys.* **2014**, *89*, 013851.
(26) Feist, A.; Echternkamp, K. E.; Schauss, J.; Yalunin, S. V.; Schafer, S.; Ropers, C. Quantum coherent optical phase modulation in an ultrafast transmission electron microscope. *Nature* **2015**, *521*, 200−203.
(27) Liebtrau, M.; Sivis, M.; Feist, A.; Lourenço-Martins, H.; Pazos-Pérez, N.; Alvarez-Puebla, R. A.; Abajo, F. J. G. d.; Polman, A.; Ropers, C. Spontaneous and Stimulated Electron-Photon Interactions in Nanoscale Plasmonic near Fields. *Light: Sci. Appl.* **2021**, *10* (1), 82−82a.
(28) Liu, H.; Baskin, J. S.; Zewail, A. H. Infrared PINEM Developed by Diffraction in 4D UEM. *Proc. Natl. Acad. Sci. U. S. A.* **2016**, *113* (8), 2041−46.
(29) Lemke, C.; Leißner, T.; Jauernik, S.; Klick, A.; Fiutowski, J.; Kjelstrup-Hansen; Rubahn, H. G.; Bauer, M. Mapping surface plasmon polariton propagation via counter-propagating light pulses. *Opt. Express* **2012**, *20*, 12877.
(30) Gennaro, S. D.; Rahmani, M.; Giannini, V.; Aouani, H.; Sidiropoulos, T. P. H.; Navarro-Cía, M.; Maier, S. A.; Oulton, R. F. The Interplay of Symmetry and Scattering Phase in Second Harmonic Generation from Gold Nanoantennas. *Nano Lett.* **2016**, *16*, 5278−5285.
(31) Wang, J.; Yu, Y.; Wei, Y.-M.; Liu, S.-F.; Li, J.; Zhou, Z.-K.; Niu, Z.-C.; Yu, S.-Y.; Wang, X.-H. High-efficiency broadband second harmonic generation in single hexagonal GaAs nanowire. *Sci. Rep.* **2017**, *7*, 2166.
(32) Li, J.; Zhang, Q.; Li, L.; Zhu, X.; Huang, T.; Lan, P.; Lu, P. Orientation dependence of high-order harmonic generation in nanowire. *Phys. Rev. A: At., Mol., Opt. Phys.* **2019**, *99*, 033421.
(33) Bernasconi, G. D.; Butet, J.; Martin, O. J. F. Mode analysis of second-harmonic generation in plasmonic nanostructures. *J. Opt. Soc. Am. B* **2016**, *33*, 768−779.
(34) de Hoogh, A.; Opheij, A.; Wulf, M.; Rotenberg, N.; Kuipers, L. Harmonics Generation by Surface Plasmon Polaritons on Single Nanowires. *ACS Photonics* **2016**, *3*, 1446−1452.
(35) Vampa, G.; Ghamsari, B. G.; Siadat Mousavi, S.; Hammond, T. J.; Olivieri, A.; Lisicka-Skrek, E.; Naumov, A. Y.; Villeneuve, D. M.; Staudte, A.; Berini, P.; Corkum, P. B. Plasmon-enhanced high-harmonic generation from silicon. *Nat. Phys.* **2017**, *13* (7), 659−662.
(36) Bautista, G.; Mäkitalo, J.; Chen, Y.; Dhaka, V.; Grasso, M.; Karvonen, L.; Jiang, H.; Huttunen, M. J.; Huhtio, T.; Lipsanen, H.; Kauranen, M. Second-Harmonic Generation Imaging of Semiconductor Nanowires with Focused Vector Beams. *Nano Lett.* **2015**, *15*, 1564−1569.
(37) Kim, S.; Jin, J.; Kim, Y.-J.; Park, I.-Y.; Kim, Y.; Kim, S.-W. High-harmonic generation by resonant plasmon field enhancement. *Nature* **2008**, *453*, 757−760.
(38) Brabec, T.; Krausz, F. Intense few-cycle laser fields: Frontiers of nonlinear optics. *Rev. Mod. Phys.* **2000**, *72*, 545−591.
(39) Konečná, A.; Di Giulio, V.; Mkhitaryan, V.; Ropers, C.; García de Abajo, F. J. Nanoscale Nonlinear Spectroscopy with Electron Beams. *ACS Photonics* **2020**, *7*, 1290−1296.
(40) Xu, Q.; Zhang, X.; Yang, Q.; Tian, C.; Xu, Y.; Zhang, J.; Zhao, H.; Li, Y.; Ouyang, C.; Tian, Z.; Gu, J.; Zhang, X.; Han, J.; Zhang, W. Polarization-controlled asymmetric excitation of surface plasmons. *Optica* **2017**, *4*, 1044.
(41) Zhang, S.; Wei, H.; Bao, K.; Hakanson, U.; Halas, N. J.; Nordlander, P.; Xu, H. Chiral surface plasmon polaritons on metallic nanowires. *Phys. Rev. Lett.* **2011**, *107*, 096801.
(42) Jackson, J. D.; Fox, R. F. Classical Electrodynamics, 3rd ed. *Am. J. Phys.* **1999**, *67*, 841−842.
(43) Schröter, U.; Dereux, A. Surface plasmon polaritons on metal cylinders with dielectric core. *Phys. Rev. B: Condens. Matter Mater. Phys.* **2001**, *64*, 125420.
(44) Chang, D. E.; Sørensen, A. S.; Hemmer, P. R.; Lukin, M. D. Strong coupling of single emitters to surface plasmons. *Phys. Rev. B: Condens. Matter Mater. Phys.* **2007**, *76*, 035420.
(45) Cai, W.; Sainidou, R.; Xu, J.; Polman, A.; García de Abajo, F. J. Efficient Generation of Propagating Plasmons by Electron Beams. *Nano Lett.* **2009**, *9*, 1176−1181.

https://doi.org/10.1021/acs.nanolett.1c03203
Nano Lett. 2021, 21, 10238−10243